

LATTICE BOLTZMANN METHOD FOR SIMULATING GAS FLOW IN MICROCHANNELS

G. H. TANG, W. Q. TAO* and Y. L. HE
School of Energy and Power Engineering
State Key Laboratory of Multiphase Flow
Xi'an Jiaotong University, Xi'an
Shaanxi 710049, P. R. China
**wqtao@mail.xjtu.edu.cn*

Received 16 August 2003
Revised 14 September 2003

Isothermal gas flows in microchannels is studied using the lattice Boltzmann method. A novel equation relating Knudsen number with relaxation time is derived. The slip-velocity on the solid boundaries is reasonably realized by combining the bounce-back reflection with specular reflection in a certain proportion. Predicted characteristics in a two-dimensional microchannel flow, including slip-velocity, nonlinear pressure drop, friction factors, velocity distribution along the streamwise direction and mass flow rate, are compared with available analytical and experimental results and good agreement is achieved.

Keywords: Flow in microchannels; lattice Boltzmann method; slip boundary condition; MEMS devices.

1. Introduction

MEMS (Micro-Electro-Mechanical-Systems) devices are becoming more prevalent in engineering applications and in scientific researches.¹ Microchannels with dimensions ranging from 100 microns to 1 micron have found many applications in areas ranging from integrated cooling of electronic circuits and flow sensors, to complex systems consisting of pumps, valves and other components.

Experimental studies for the flow measurements in microchannels have been conducted and the results are quite contradictory. The measured friction factor by Wu and Little² are much higher than those predicted by the Moody chart, while the friction factor measured in Refs. 3–5 are lower than the conventional ones. In addition, Shih *et al.*⁶ and Turner *et al.*⁵ measured the local pressure distribution of nitrogen and helium along the channel length and the nonlinear pressure distributions were clearly observed.

*Corresponding author.

One reason accounting for the contradictory test results in the friction factor is associated with the obvious measurement difficulties. Numerical analysis, however, provides an alternative and effective way for investigating the flow inside a microchannel or a more complex geometry.

Arkilic *et al.*⁷ developed a two-dimensional model for rarefied gas flow through microchannels by solving the Navier–Stokes equations with a first-order slip-velocity boundary condition. Chen *et al.*⁸ numerically solved the two-dimensional, compressible Navier–Stokes equations along with a first-order slip-velocity boundary condition for gaseous flow in a microchannel. For the case of Knudsen number larger than 0.1 in which slip flow approximation is not valid, the direct simulation-Monte Carlo (DSMC) is used for investigating the flow characteristics in microchannels.⁹ Since in the DSMC method the number of particles distributed in the field is directly related to the number of molecules, the computational effort is usually very large. Another numerical simulation method in the meso-scale level, the lattice Boltzmann method, provides an alternative simulation tool for the microchannel flows covering different flow regimes.

Since 1980s, the lattice Boltzmann method (LBM) has been widely used for many kinds of continuum viscous flows that are difficult to deal with for conventional numerical approaches.¹⁰ Unlike traditional kinetic methods and the DSMC method, this model solves a simplified Boltzmann equation on regular lattices. The LBM method has been mainly applied to the continuum flow regime since its birth. Very recently, Nie *et al.*¹¹ and Lim *et al.*¹² have tried to use LBM to simulate microflows and generated some promising results. In Ref. 11 a two-dimensional microchannel flow was simulated with bounce-back boundary treatment. Lim *et al.*¹² linked the relaxation time τ with the molecular free mean path λ based on an assumption of $\lambda = \tau\Delta x$, where Δx is the lattice spacing. Therefore, the Knudsen number can be computed as $Kn = \lambda/H = \tau/N_y$, where N_y is the number of lattice units in the y -direction.

The simulation of the microchannel flow by the lattice Boltzmann method is in its infancy and many issues are worthy of further investigation. The aim of the present paper is three-fold. First to investigate the relation between the Knudsen number and the relaxation time from the basic consideration of gas kinematics, and a new relation between Kn and τ is derived; second, the wall slip boundary condition is treated by a combination of specular boundary and bounce-back treatment based on some observable results of gas kinematics. Third, these two new treatments of the lattice Boltzmann methods are used in a simulation of gas flow in 2D microchannels and the results are compared with available experimental and analytical data.

2. Lattice Boltzmann Model

The discrete lattice Boltzmann equation with the BGK collision approximation can be written as¹³

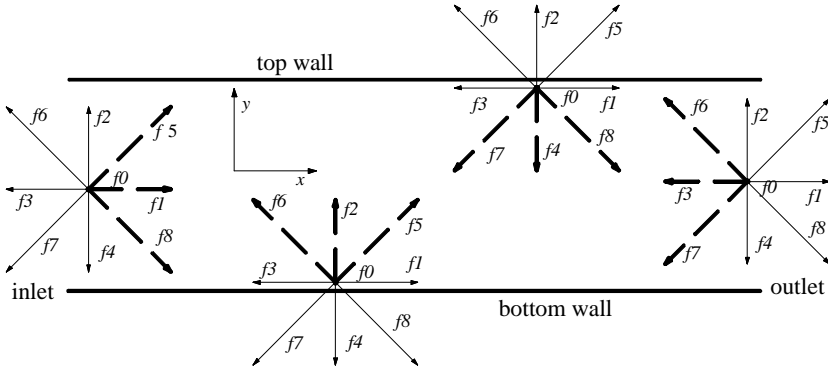


Fig. 1. The D2Q9 lattice and particle distributions at boundaries.

$$f_i(\mathbf{r} + \mathbf{c}_i \Delta t, t + \Delta t) = f_i(\mathbf{r}, t) - \frac{1}{\tau} [f_i(\mathbf{r}, t) - f_i^{\text{eq}}(\mathbf{r}, t)]. \tag{1}$$

The parameter \mathbf{c}_i is the particle discrete velocity. For a square lattice D2Q9 model as shown in Fig. 1, $\mathbf{c}_0 = 0$ corresponds to the distribution with zero velocity, $\mathbf{c}_i = (\cos[(i-1)\pi/2], \sin[(i-1)\pi/2])c$ for $i = 1, 2, 3, 4$, and $\mathbf{c}_i = (\cos[(i-5)\pi/2 + \pi/4], \sin[(i-5)\pi/2 + \pi/4])c$ for $i = 5, 6, 7, 8$, where $c = \Delta x / \Delta t$ is the particle streaming speed, and $\Delta x, \Delta t$ are the lattice spacing and step size in time, respectively.

In Eq. (1) f_i^{eq} ($i = 0, 1, \dots, 8$) stands for the equilibrium density distribution function and for the D2Q9 lattice, one obtains the following form¹⁴

$$f_i^{\text{eq}} = \rho \omega_i \left[1 + \frac{3(\mathbf{c}_i \cdot \mathbf{u})}{c^2} + \frac{9(\mathbf{c}_i \cdot \mathbf{u})^2}{2c^4} - \frac{3(\mathbf{u} \cdot \mathbf{u})}{2c^2} \right], \tag{2}$$

where $\omega_0 = 4/9$, $\omega_i = 1/9$ for $i = 1, 2, 3, 4$, and $\omega_i = 1/36$ for $i = 5, 6, 7, 8$. The macroscopic variables such as mass density and the momentum density are defined by sums over the distribution functions $f_i(\mathbf{r}, t)$

$$\rho = \sum_i f_i, \quad \rho \mathbf{u} = \sum_i f_i \mathbf{c}_i, \quad p = \frac{c^2}{3} \rho. \tag{3}$$

In traditional lattice-BGK models, τ is chosen to be a constant. This is applicable only for nearly incompressible fluids. In micro-flows, the density difference could be quite large. Therefore, Nie *et al.*¹¹ replaced τ with τ' to include the dependence of viscosity on density.

$$\tau' = \frac{1}{2} + \frac{1}{\rho} \left(\tau - \frac{1}{2} \right). \tag{4}$$

Application of the multi-scale technique (Chapman–Enskog expansion) yields the Navier–Stokes equation with pressure $p = \rho k_B T / m$, where $m = \text{const}$ represents the particle mass, and dynamic viscosity

$$\eta = \frac{c^2(\tau - 0.5)\Delta t}{3}. \tag{5}$$

One can see Ref. 11 for detailed derivation of the dynamic viscosity. For a specific computation, c , Δt and τ remain unchanged, therefore, the dynamic viscosity of the fluid simulated keeps constant which is required for most realistic fluids.

Nie *et al.*¹¹ defined the relation between the Knudsen number and the relaxation parameter by the following form

$$Kn = \frac{\alpha(\tau - 0.5)}{\rho N_y}. \quad (6)$$

The coefficient α was chosen to be 0.388 to best match the simulated mass flow rate with experimental data for flow in a microchannel with a high aspect ratio. The bounce-back boundary condition was implemented at the top and bottom plates. It can be seen that the value of α in Nies' model is empirical in nature. It is our consideration that a more general expression between Kn and τ should be derived based on the gas kinematics without introducing such empirical coefficient.

To proceed, let us review some basic concept of the gas kinetics. For gases, the mean free path λ is the average distance traveled by molecules between collisions. For an ideal gas modeled as rigid spheres, the mean free path is related to temperature T and pressure p as follows¹⁵

$$\lambda = \frac{k_B T}{\sqrt{2} \pi \rho \sigma^2}, \quad (7)$$

where σ is the molecular diameter, and k_B is the Boltzmann constant.

From the kinetic theory of gases, the mean free path is related to the dynamic viscosity by

$$\eta = \frac{1}{2} \lambda \rho \bar{v}_m, \quad (8)$$

where \bar{v}_m is the mean molecular speed which is calculated by

$$\bar{v}_m = \sqrt{\frac{8k_B T}{\pi m}}. \quad (9)$$

The density is determined as

$$\rho = \frac{mp}{k_B T}. \quad (10)$$

From Eqs. (8)–(10), the following relation can be derived

$$\lambda = \frac{\eta}{p} \sqrt{\frac{\pi k_B T}{2m}}. \quad (11)$$

Therefore, the ratio of the mean free path to the characteristic length, i.e., the Knudsen number, is

$$Kn = \frac{\lambda}{H} = \frac{\eta}{pH} \sqrt{\frac{\pi k_B T}{2m}}. \quad (12)$$

Since the Knudsen number changes along the microchannel in most cases, and the outlet condition is known (usually at atmospheric condition), the channel outlet

temperature and pressure are adopted. First we used another form of Eq. (4) for perspicuity

$$\tau' = \frac{1}{2} + \frac{\rho_{\text{ref}}}{\rho} \left(\tau - \frac{1}{2} \right), \quad (13)$$

where ρ_{ref} is the constant referenced mass density. Then Eq. (5) becomes

$$\eta = \frac{\rho_{\text{ref}} c^2 (\tau - 0.5) \Delta t}{3}. \quad (14)$$

Substituting Eq. (14) into Eq. (12) (since the idea behind the lattice Boltzmann method is to construct a simplified molecular dynamics model that incorporates many of the essential characteristics of the real microscopic process, the macroscopic averaged properties of the predicted results obey the desired macroscopic equations,¹⁰ it is reasonable to relate the mean free path with the dynamic viscosity in the discrete lattice Boltzmann equation), and assuming a uniform mesh and isothermal flow, we yield the following result after a lengthy derivation

$$Kn_0 = \sqrt{\frac{\pi}{24}} \frac{(2\tau - 1)\rho_{\text{ref}}}{\rho_0 N_y} \quad \text{or} \quad \tau = \frac{\rho_0 N_y Kn_0}{\rho_{\text{ref}} \sqrt{\pi/6}} + \frac{1}{2}, \quad (15)$$

where Kn_0 is the Knudsen number at the outlet of the channel. It should be noted that the derived constant coefficient of Eq. (15) differs from Eq. (6). This phenomenon may be explained due to different boundary treatment methods discussed in the following sections. Based on the isothermal assumption, the product of pressure and Knudsen number should be constant along the channel. Then the local Knudsen number is related to Kn_0 as follows

$$Kn = \frac{Kn_0}{P(x)}, \quad (16)$$

where the local dimensionless pressure $P(x)$ is defined as the ratio of the local pressure to the outlet pressure.

Attention is now turned to the boundary condition treatment. In the lattice gas automata, the so-called “nonslip” boundary condition, namely zero fluid velocity at a given solid surface is obtained with bounce-back reflection. Free-slip boundary condition applies to the case of smooth boundaries with negligible friction exerted upon the flowing gas or liquid. In this case, the tangential motion of the fluid flow on the wall is free and no momentum is to be exchanged with the wall along the tangential component. Specular reflection is applied to obtain free-slip boundary condition in lattice Boltzmann method. For real gas flow in microchannels, neither pure no-slip bounce-backs nor pure free-slip specular reflections can appropriately describe the momentum exchange and friction drag between the wall and the fluid. Thus some combination of them is considered a better way to simulate the actual boundary condition of gas flow in microchannels.

Another reason of this consideration stems from the experiment at the molecular level described by Knudsen.¹⁵ In an experiment where molecules are directed

towards a wall at a fixed angle of incidence, he observed that the molecules are randomly scattered in all directions. In the lattice gas automata, this would correspond to a combination of specular and bounce-back reflections in equal proportions, i.e., $r_b = 0.5$.

We define a reflection coefficient r_b as the proportion of bounce-back reflections in the interactions with the wall and $1 - r_b$ represents the specular reflections proportion. Therefore, $r_b = 1$ corresponds to pure bounce-back reflection and $r_b = 0$ to pure specular reflection. For the bottom and top wall, the boundary conditions are given in the following forms (Fig. 1):

At bottom wall

$$\begin{aligned} f_2(x, 0) &= f_4(x, 0), \\ f_5(x, 0) &= r_b f_7(x, 0) + (1 - r_b) f_8(x, 0), \\ f_6(x, 0) &= r_b f_8(x, 0) + (1 - r_b) f_7(x, 0). \end{aligned} \quad (17a)$$

At top wall

$$\begin{aligned} f_4(x, H) &= f_2(x, H), \\ f_7(x, H) &= r_b f_5(x, H) + (1 - r_b) f_6(x, H), \\ f_8(x, H) &= r_b f_6(x, H) + (1 - r_b) f_5(x, H). \end{aligned} \quad (17b)$$

After the particle's collision with the wall, the normal momentum component at the bottom wall can be determined as follows:

$$J_y(x, 0) = f_2 - f_4 + f_5 - f_8 + f_6 - f_7. \quad (18)$$

By substituting Eq. (17a), we yield $J_y(x, 0) = 0$. This expression implies that the normal velocity component vanishes, namely, no motion normal to the wall.

Due to the collapse of continuous assumption for the case of large Kn number, a slip velocity appears even when the pure bounce-back reflection treatment is adopted as indicated in Ref. 11, therefore $r_b = 0.5$ seems to over-predict the slip velocity. Compared with results from Arkilics' model, $r_b = 0.7$ is used to best capture the slip-velocity on the solid-gas wall, which means that more fluid particles will be reflected in the backward direction than the forward direction. Probably, the value of r_b is Kn number dependent. For the present Kn number range (0.055–0.16) this value works well. Further work is underway in the authors' group in order to reveal the relation between Kn and r_b . In our work, the pressure or density values at the inlet and outlet are fixed, and velocity components are extrapolated from downstream and upstream, respectively. Thus the three unknown distributions f_1 , f_5 , f_8 at the inlet and f_3 , f_6 , f_7 at the outlet can be obtained.¹²

In the following sections, the isothermal microflows between two plane plates are investigated with the lattice Boltzmann method mentioned above. The length of the channel is 100 times of the height except for specially noted cases, and outlet Knudsen number is 0.16 for helium and 0.055 for nitrogen at atmospheric outlet condition. The corresponding channel height is 1.2 microns.

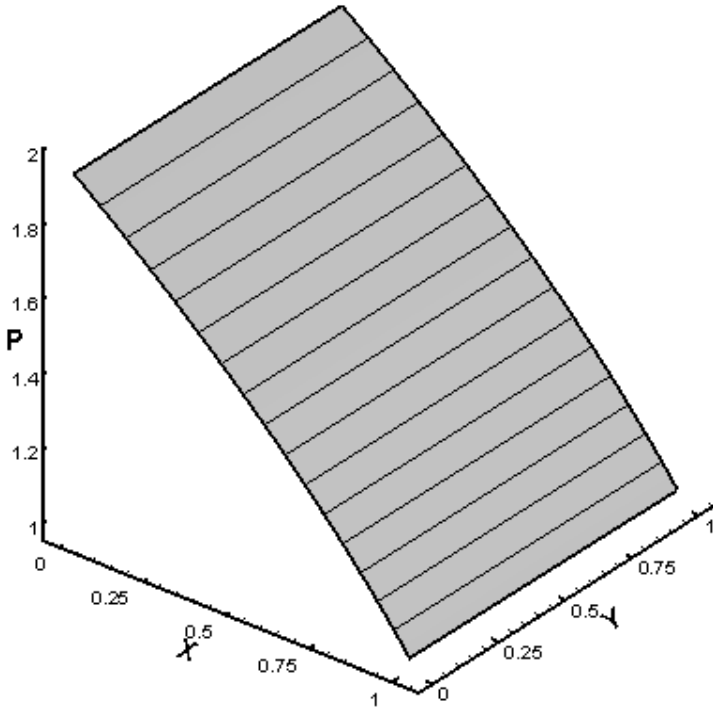


Fig. 2. Pressure distributions in the channel.

3. Results and Discussion

Figure 2 shows the normalized pressure distribution along the channel ($P_i = 1.94, Kn_0 = 0.055$). It can be seen that P is only dependent on normalized location X , and it remains unchanged across the channel. Figures 3 and 4 illustrate the tangential and normal velocity components normalized by the particle streaming speed, respectively. From the figures, the following features may be noted. First the slip-velocity at the wall and the centerline velocity increase markedly toward the exit. This is required by the constraint of mass conservation since the pressure decreases along the channel. Second, the U -velocity profile across the channel is of parabolic type and is symmetrical throughout. Third, the magnitude of the V -velocity profile is of several orders smaller than that of U . These results qualitatively agree well with those from previous studies (Arkilic *et al.*⁷ and Lim *et al.*¹²).

Deviations from linear pressure drop (i.e., corresponding to incompressible laminar flow) for different inlet pressures with the same outlet Knudsen number are shown in Fig. 5. Here the vertical coordinate of the plot is expressed as $P' = (p - p_{\text{linear}})/p_0$. We can observe that for the same outlet Knudsen number $Kn_0 = 0.055$, the increase in the inlet pressure, i.e., the increase in compressibility within the channel, results in a larger deviation from the linear pressure distribution

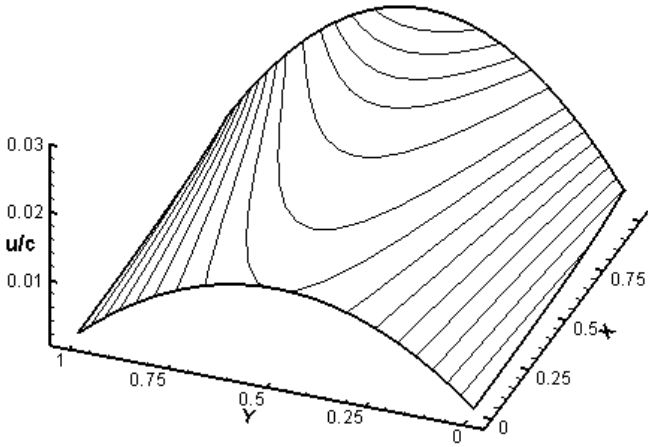


Fig. 3. U -velocity distributions in the channel.

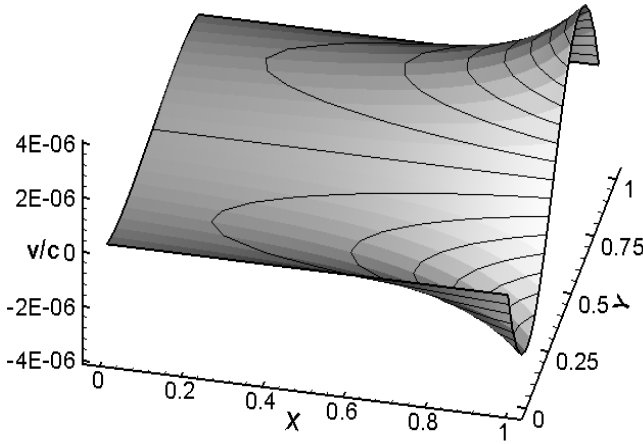


Fig. 4. V -velocity distributions in the channel.

expected in an incompressible channel flow. Furthermore, the location of maximum deviation from linear pressure distribution moves toward the channel exit as the inlet pressure increases. In Fig. 5, our results agree well with Arkilics' model in the locations of the maximum deviation from linear pressure.

The effects of different outlet Knudsen number are shown in Fig. 6. There $Kn_0 = 0.062$ stands for argon flow in the channel at the same condition. For different Kn_0 cases, it can be observed that the stronger the rarefaction effects, as indicated by the larger value of Kn_0 , the smaller the deviation from the linear pressure distribution. This means that the rarefaction effects serve to decrease the curvature in the pressure distribution caused by the compressibility effect. Thus the effect of the compressibility and the effect of the rarefaction on the pressure distribution are

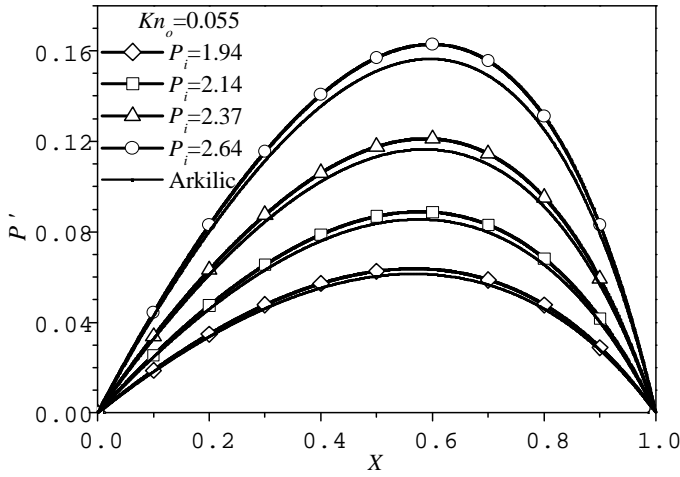


Fig. 5. Nonlinearity of pressure along the channel.

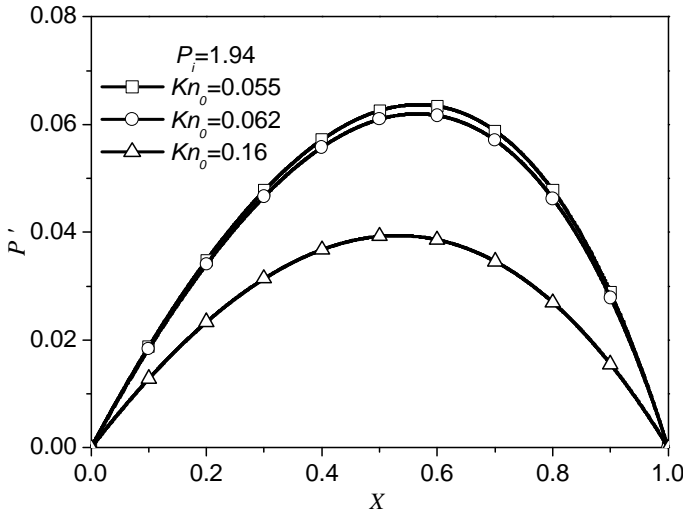


Fig. 6. Nonlinearity of pressure for different Knudsen numbers.

contradictory. The final distribution of the pressure along the channel is somewhat balance between these two effects. Generally speaking, the two effects are not equal, resulting in a nonlinear pressure distribution.

The local Knudsen numbers along the streamwise direction are shown in Fig. 7. As can be observed Kn is a function of the local pressure (see Eq. (14)). With the decreasing pressure along the channel, the Knudsen number increases and reaches its maximum value at the outlet. The results from our LBM analysis agree well with the experimental ones in Ref. 6.

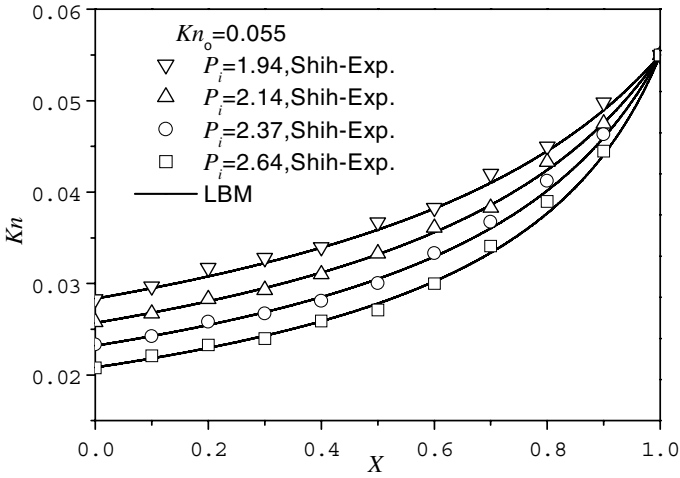


Fig. 7. Local Knudsen number distributions along the channel.

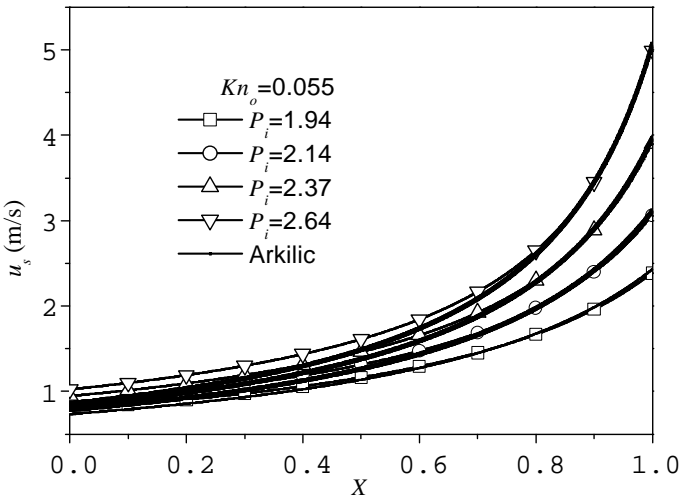


Fig. 8. Slip-velocity distributions along the wall.

In Fig. 8, the variation of slip-velocity along the length of the wall is presented. Due to the pressure drop along the channel, the local Knudsen number increases correspondingly, resulting in an accompanying increase in the slip-velocity in the streamwise direction. In our simulation results, the magnitude and variation trend of the slip-velocity agree well with Arkilic’s model when $r_b = 0.7$.

The comparisons of average friction factors predicted from the present LBM analysis with those from other methods (including Arkilic’s model and experiments) are presented in Fig. 9. The theoretical friction factor for fully developed incompressible flow is used for normalizing C^* , $C^* = f/f_{\text{theory}}$. The present results agree

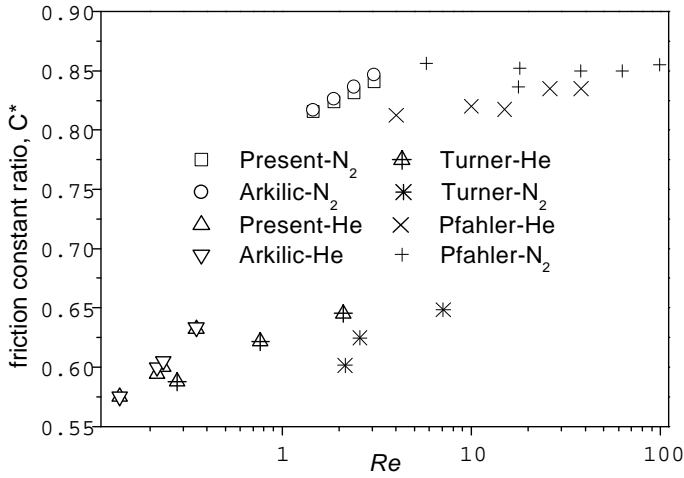


Fig. 9. Comparisons of average friction factors.

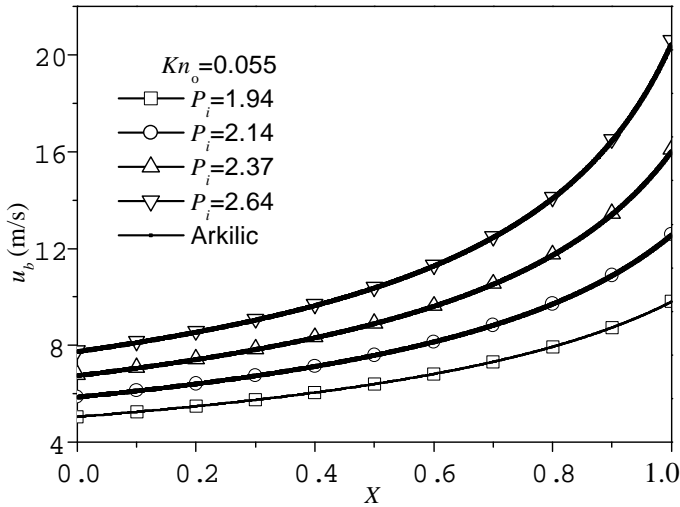


Fig. 10. Bulk u -velocities along the channel for nitrogen.

well with those predicted by Arkilics' model. The predicted results for helium seem to be more agreeable with Turners' experiments while the predicted nitrogen results are close to the experimental data of Pfahlers'.

Figure 10 shows the average velocity variations along the streamwise direction. As the flow proceeds down the channel, the pressure drops and consequently, to preserve mass continuity, the average velocity increases. The predicted results of the present study and those of Arkilics' are too close to be plotted as separated curves.

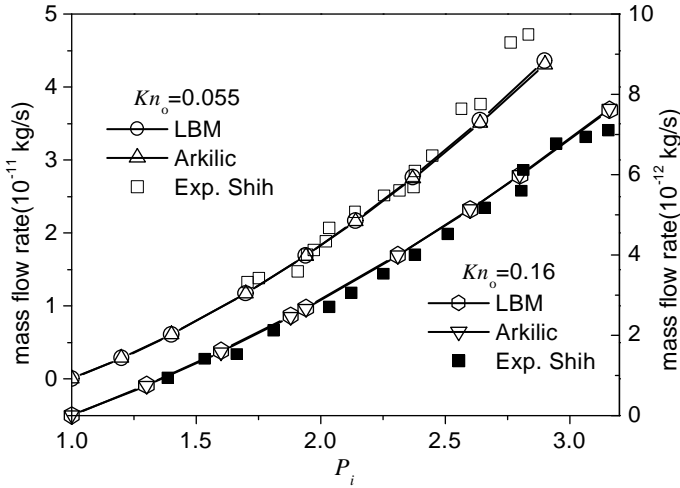


Fig. 11. Mass flow rates for different inlet pressure ratios.

Finally, we plot the mass flow rate as a function of the inlet to outlet pressure ratio in Fig. 11 and compared it with Arkilics' model and experiments. The height, width and length of the channel in simulation are set to be 1.2 microns, 40 microns and 3600 mm, respectively, which are the real parameters in Shihs' experiments.⁶ The outlet Knudsen number is 0.055 for nitrogen and 0.16 for helium. As shown, present model gives a good matching with the Arkilics' model. The experimental data scatter around the prediction line in a satisfaction degree within the range of $1 \leq P_i \leq 2.5$ for nitrogen and within the range of $1 \leq P_i \leq 3.2$ for helium.

4. Conclusions

The lattice Boltzmann method (LBM) is adopted with some modifications to simulate two-dimensional isothermal microchannel flow. A novel method relating the Knudsen number Kn with the relaxation time τ is derived. In addition, to capture the slip velocity on the solid boundaries more appropriately, a scheme of combining the bounce-back reflection with specular reflection is proposed and applied to boundary condition treatment. Characteristics in the two-dimensional microchannel flow including slip-velocity, nonlinear pressure drop, friction coefficient, average velocity along the streamwise direction and mass flow rate are compared with those from Arkilics' model and the available experimental data, and the agreements are quite well, showing that the lattice Boltzmann method is a promising approach for simulating the flow in microchannels.

The present model is verified to be more advantageous because we only need to decide the proportion of bounce-back reflections r_b and the predicted flow results are shown to be more close to the available data as well. Furthermore, the present model together with the chosen $r_b = 0.7$ is confirmed to have a fairly strong

applicability to a wide range of Knudsen number ($K_n = 0.055\text{--}0.16$) and pressure ratio ($P_i = 1.0\text{--}3.0$), which accord with the general encountered situations in microflow applications.

Acknowledgments

The authors would like to thank Professor C. Shu for the discussion over this work. This work was supported by the National Fundamental R&D Project of China (No. G2000026303), the National Natural Science Foundation of China (Nos. 50076034, 50236010) and the Doctoral Foundation of Xi'an Jiaotong University (No. DFXJTU2002-1).

References

1. M. Gad-el-Hak, *J. Fluids Eng.* **121**, 5 (1999).
2. P. Y. Wu and W. A. Little, *Cryogenics* **23**, 273 (1983).
3. J. Pfahler, J. Harley, H. H. Bau and J. N. Zemel, *ASME, DSC-Vol.* **32**, 49 (1991).
4. S. B. Choi, R. F. Barron and R. O. Warrington, *ASME, DSC-Vol.* **32**, 123 (1991).
5. S. E. Turner, H. W. Sun and M. Faghri, *ASME, HTD-Vol.* **364-3**, 71 (1999).
6. J. C. Shih, C. M. Ho, J. Q. Liu and Y. C. Tai, *ASME, DSC-Vol.* **59**, 197 (1996).
7. E. B. Arkilic, M. A. Schmidt and K. S. Breuer, *J. Microelectromechanical Syst.* **6**, 167 (1997).
8. C. S. Chen, S. M. Lee and J. D. Sheu, *Numer. Heat Transf., Part A* **33**, 749 (1998).
9. G. A. Bird, *Molecular Gas Dynamics and the Direct Simulation of Gas Flows* (Oxford University Press, New York, 1994).
10. S. Y. Chen and G. D. Doolen, *Annu. Rev. Fluid Mech.* **30**, 329 (1998).
11. X. B. Nie, G. D. Doolen and S. Y. Chen, *J. Stat. Phys.* **107**, 279 (2002).
12. C. Y. Lim, C. Shu, X. D. Niu and Y. T. Chew, *Phys. Fluids* **14**, 2299 (2002).
13. S. Succi, *Lattice Boltzmann Equation for Fluid Dynamics and Beyond* (Clarendon Press, Oxford, 2001).
14. D. A. Wolf-Gladrow, *Lattice-Gas Cellular Automata and Lattice Boltzmann Models: An Introduction* (Springer, Berlin, 2000).
15. M. Knudsen, *The Kinetic Theory of Gases* (Methuen Monographs, London, 1934).